Chimoto *et al. Earth, Planets and Space* (2016) 68:206
DOI 10.1186/s40623-016-0581-3

Earth, Planets and Space

LETTER Open Access

Estimation of shallow S-wave velocity structure using microtremor array exploration at temporary strong motion observation stations for aftershocks of the 2016 Kumamoto earthquake

Kosuke Chimoto[1*], Hiroaki Yamanaka[1], Seiji Tsuno[2], Hiroe Miyake[3] and Nobuyuki Yamada[4]

Abstract

Shallow S-wave velocity V_S profiles were estimated for 26 temporary strong motion observation sites surrounding the epicenters of a sequence of the 2016 Kumamoto earthquake. The microtremor array method was used to gather the dispersion characteristics of Rayleigh waves. V_S profiles were obtained by inverting the dispersion curves for each site and those of three permanent strong motion stations that recorded the sequence of seismic events. The shallow V_S profiles near two of the permanent strong motion stations in the town of Mashiki were almost identical. However, the V_S profiles at other stations varied. The V_S profiles were found to have the common feature of the uppermost low-velocity layer being widely distributed from Mashiki to the village of Minami-Aso, and it was especially thick in the areas that suffered heavy damage. This low-velocity layer was a major contributor to the site amplification. The horizontal-to-vertical spectral ratios of the microtremors indicate that both the shallow soil and deep sedimentary layers may control the site response characteristics over a broad frequency range.

Keywords: Shallow S-wave velocity structure, Microtremor array exploration, 2016 Kumamoto earthquake, Site amplification

Background

This study focuses on the measurement of the S-wave velocity V_S of near-surface materials at temporary strong motion stations of the 2016 Kumamoto earthquake by Yamanaka et al. (2016). Temporary stations were established immediately after the M_j 7.3 event occurred on 16 April 2016 to observe the strong motion of aftershocks and investigate the cause of the heavy damage at 26 sites in a wide area along the Futagawa and Hinagu fault zones. They successfully obtained many strong motion records and showed that the records varied significantly even when the station separation was small, and strong local site effects were observed at the temporary stations installed at sites experiencing heavy damage. To provide better insight into the variety of ground motions, the dynamic response characteristics of the shallow soil must be investigated, since the characteristics of the near-surface soil have a major influence on the ground motion (e.g., Borcherdt 1970) and the resulting damage (e.g., Takeyama et al. 1960). V_S profiling is an important method of understanding site response characteristics. It can be used not only to understand the variation in aftershock records but also to estimate the strong ground motion that occurs during the event and how it contributes to the distribution of damage (e.g., Kudo et al. 2002).

The target area for the aftershock observation has a varying surface geology (Editorial Meeting of Geologic map of Kumamoto 2008). An extension of the Futagawa fault, which caused the M_j 7.3 event on April 16, 2016, exists in the southwestern part of the city of Kumamoto,

*Correspondence: chimoto.k.aa@m.titech.ac.jp
[1] Tokyo Institute of Technology, Tokyo, Japan
Full list of author information is available at the end of the article

which is located on the alluvial plane. The center of the town of Mashiki, an area that experienced heavy damage, is located on a terrace with early Pleistocene pyroclastic sediments (Editorial Meeting of Geologic map of Kumamoto 2008). However, there is insufficient information on the detailed V_S profile, which is an effective parameter for site amplification. The microtremor exploration method is now widely used for V_S profiling because it is also non-invasive and cost-effective (Okada 2003). It is recognized as a useful technique to obtain site response characteristics (Kudo et al. 2002).

In this study, microtremor array exploration was performed, and the V_S profiles at the temporary stations were obtained and described. The site response and damage characteristics caused by the event are discussed in this paper based on the measured V_S profiles. Since the present measurement site also includes three permanent stations that observed the M_j 7.3 event, the results of this study could be useful in future studies on strong motion records.

Microtremor array measurements

Microtremor array measurements were conducted at 26 temporary aftershock observation stations to evaluate site response characteristics. The stations established by Yamanaka et al. (2016) are widely distributed in the area surrounding the epicenters of a sequence of the 2016 Kumamoto earthquake, as shown in Fig. 1 and Table 1.

The microtremor records were measured using seven sets of vertical seismometers and loggers, which were deployed in a double triangular array around the center of the triangles (Kudo et al. 2002). Microtremor array records were observed for approximately 10–20 min at each site. Arrays ranging in size from 1.5 to 30 m were constructed depending on the available space, as described in Table 1. A high-damping moving coil-type seismometer (JEP6A3, Mitutoyo Corp.) connected to a wireless data logger with 24-bit accuracy (SU101, Hakusan Corp.) was used with a sampling rate of 100 Hz (Grutas and Yamanaka 2012).

It is recognized that during and after strong shaking, the velocity of the soil decreases (Pavlenko and Irikura 2006; Sawazaki et al. 2009; Hobiger et al. 2016). However, it is unknown how much temporal change in velocity for shallow soil occurred due to this event, and how much recovered from the temporal change at the moment for the measurements of microtremors, which

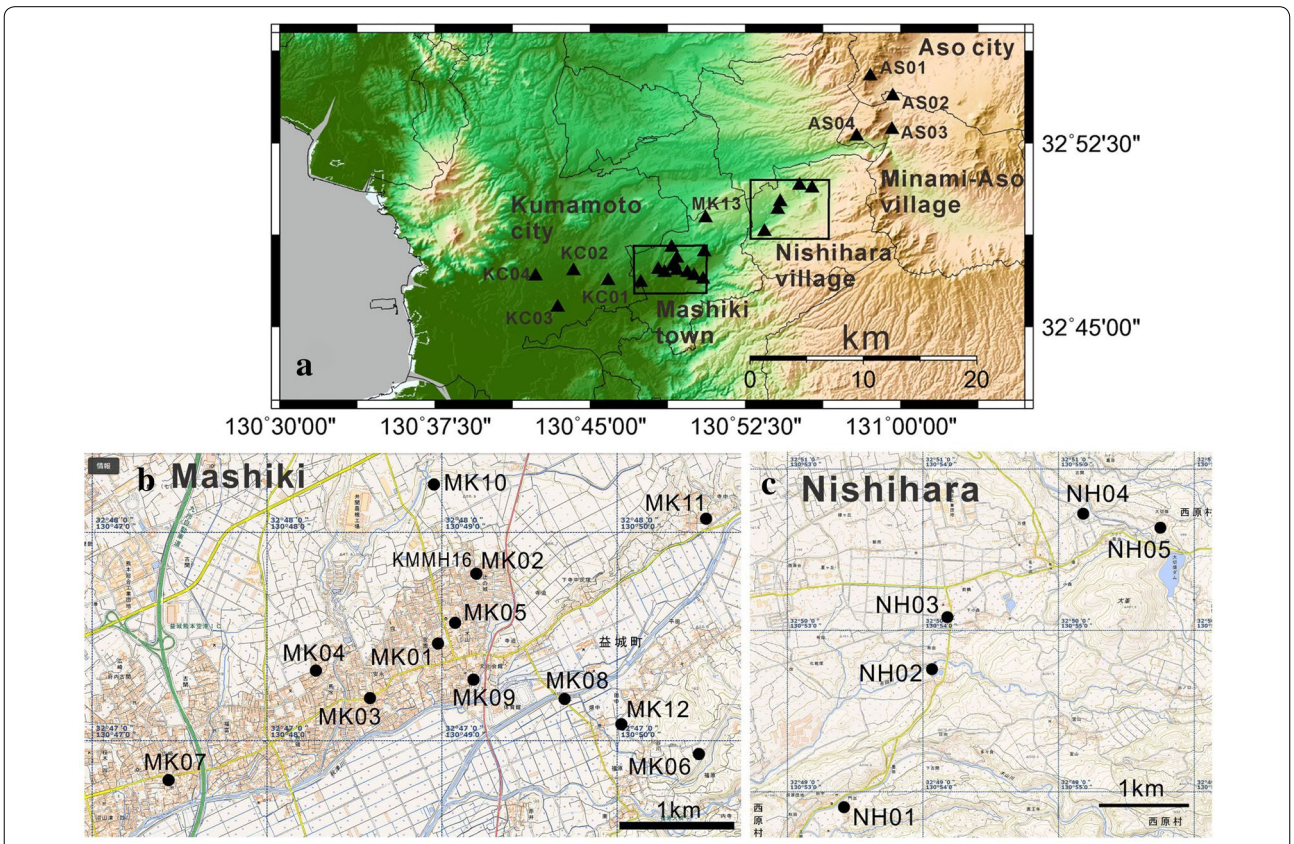

Fig. 1 **a** Location of microtremor array exploration performed near the temporary stations established by Yamanaka et al. (2016). Enlarged views of **b** Mashiki and **c** Nishihara

Table 1 Sites of microtremor array measurements, size of array and obtained AVS30 values

Region	Site code	Lat. (deg.)	Long. (deg.)	Date in 2016	Array size[a] (m)	AVS30 ± SD (m/s)
Aso and Minami-Aso	AS01	32.920410	130.975480	22 May	13–2	495 ± 0.31
	AS02	32.906830	130.993700	22 May	13–2	267 ± 0.69
	AS03	32.884100	130.992940	22 May	12–1.5	254 ± 0.49
	AS04	32.879480	130.964540	22 May	20–2.5	401 ± 0.35
Kumamoto city	KC01	32.781222	130.764500	1 May	30–3	259 ± 0.30
	KC02	32.787970	130.736510	20 May	12–1.5	313 ± 1.61
	KC03	32.763166	130.723796	20 May	20–2.5	194 ± 0.85
	KC04	32.784400	130.706020	20 May	20–2.5	232 ± 0.98
Mashiki	MK01	32.791222	130.816194	21 May	4–2	258 ± 0.63
	MK02	32.796639	130.819806	21 May	20–2.5	248 ± 0.68
	MK03	32.786750	130.809833	1 May	8–1.5	244 ± 1.40
	MK04	32.789056	130.804778	30 April	5–1.5	267 ± 1.37
	MK05	32.792750	130.817639	1 May	9–1.5	241 ± 1.28
	MK06	32.782306	130.841056	21 May	8–1.5	261 ± 0.97
	MK07	32.780250	130.790667	30 April	10–1.5	229 ± 1.30
	MK08	32.786722	130.828361	30 April	7–2	309 ± 0.22
	MK09	32.788194	130.819722	30 April	14–2	252 ± 2.00
	MK10	32.804000	130.815611	30 April	6–1.5	284 ± 1.94
	MK11	32.800833	130.841833	30 April	12–1.5	330 ± 0.98
	MK12	32.784667	130.833667	21 May	20–2.5	335 ± 0.21
	MK13	32.823891	130.842807	21 May	24–3	269 ± 1.04
Nishihara	NH01	32.814820	130.890180	22 May	12–1.5	410 ± 0.11
	NH02	32.829620	130.901050	21 May	20–2.5	339 ± 0.41
	NH03	32.834950	130.903080	22 May	11–1.5	256 ± 0.32
	NH04	32.846089	130.918586	21 May	16–2	270 ± 0.72
	NH05	32.844250	130.928800	21 May	10–1.5	231 ± 1.04

[a] Maximum and minimum side length of triangles

was performed more than 2 weeks after the events had occurred (Table 1). The influence of the possible velocity decrease on *Vs* profiling will be discussed later.

Estimation of phase velocity

The phase velocity dispersion curve was estimated using the spatial autocorrelation (SPAC) method (Okada 2003). The microtremor records were first divided into segments with equal timespans of 20.48 s each. The SPAC coefficients were calculated in each window for smoothed spectra using a Parzen window with the bandwidth varying from 0.5 to 2.0 Hz depending on the array size. The calculated SPAC coefficients were obtained as averages over these 20.48 s segments, excluding outlier SPAC coefficient values. The phase velocity curve was estimated by fitting the SPAC coefficients to the zero-order Bessel function of the first kind assuming that the microtremors are mainly surface waves of fundamental-mode Rayleigh waves.

Figure 2a compares the phase velocity dispersion curves estimated near the two permanent strong motion stations in Mashiki, MK01 and MK02, which recorded a sequence of events during the 2016 Kumamoto earthquake. The two dispersion curves obtained at MK01 and MK02, which are separated by a distance of approximately 700 m, were found to be consistent with each other. The gray line shows the dispersion curve calculated for the soil model at KMMH16 determined by the National Research Institute for Earth Science and Disaster Prevention (NIED) from borehole logging. The difference between the phase velocity curves calculated for KMMH16 and observed at MK02, where a temporary station was installed near KMMH16 by Yamanaka et al. (2016), was significant in the frequency range of approximately 6–20 Hz. Figure 2b and c show the dispersion curves at the other sites in Mashiki categorized by the degree of damage around the temporary stations. The damage at the temporary sites has been reported by Yamanaka et al. (2016). The phase velocity curves at the sites experiencing heavy and moderate damage are shown in Fig. 2b. The curves have the common feature of a low velocity even in the low frequency range. MK05, which is located between MK01 and

MK02, showed dispersive features different from those at these two sites, despite the fact that they were consistent with each other. The sites experiencing slight damage, MK06, MK08, MK11, and MK12, which are located in the southeastern part of the target area in Mashiki, showed large phase velocity curves (Fig. 2c). MK04 also has a large phase velocity and is located in the northern part, where the damage was slight compared with that at the strong motion station sites.

The phase velocity curves from the other areas are shown in Fig. 2d–f. The phase velocity curves in the western part of the Aso region are plotted in Fig. 2d. The site AS03 is located in the district closest to the collapsed Aso Bridge, where many apartments collapsed. The dispersion curve at AS03 has one feature similar to those obtained at the sites experiencing heavy damage in Mashiki (Fig. 2b): It showed a constant velocity of 100 m/s at frequencies above 10 Hz and significant dispersion below 10 Hz. In the central part of Kumamoto, a non-dispersive trend was observed above 4 and 6 Hz at KC03 and KC04, respectively, with a velocity of approximately 150 m/s (Fig. 2e). The phase velocity curves obtained in the village of Nishihara are shown in Fig. 2f. The site NH03 is located near a permanent station that recorded a larger peak ground velocity than in Mashiki during the M_j 7.3 event on April 16, 2016. The phase velocity curve at NH03 showed characteristics similar to those of the curve at MK01 in that the velocity at frequencies above 10 Hz was approximately 100 m/s and showed significant dispersion below 10 Hz. The curve at NH05 exhibited the slowest velocity at low frequencies among the sites in Nishihara; many wooden houses collapsed, and ground failure occurred near this site.

Inversion of phase velocity

The Rayleigh wave phase velocity curves were inverted for the S-wave velocity using the hybrid heuristic inversion technique, which applies a genetic algorithm and simulated annealing (Yamanaka 2007; Takekoshi and Yamanaka 2009).

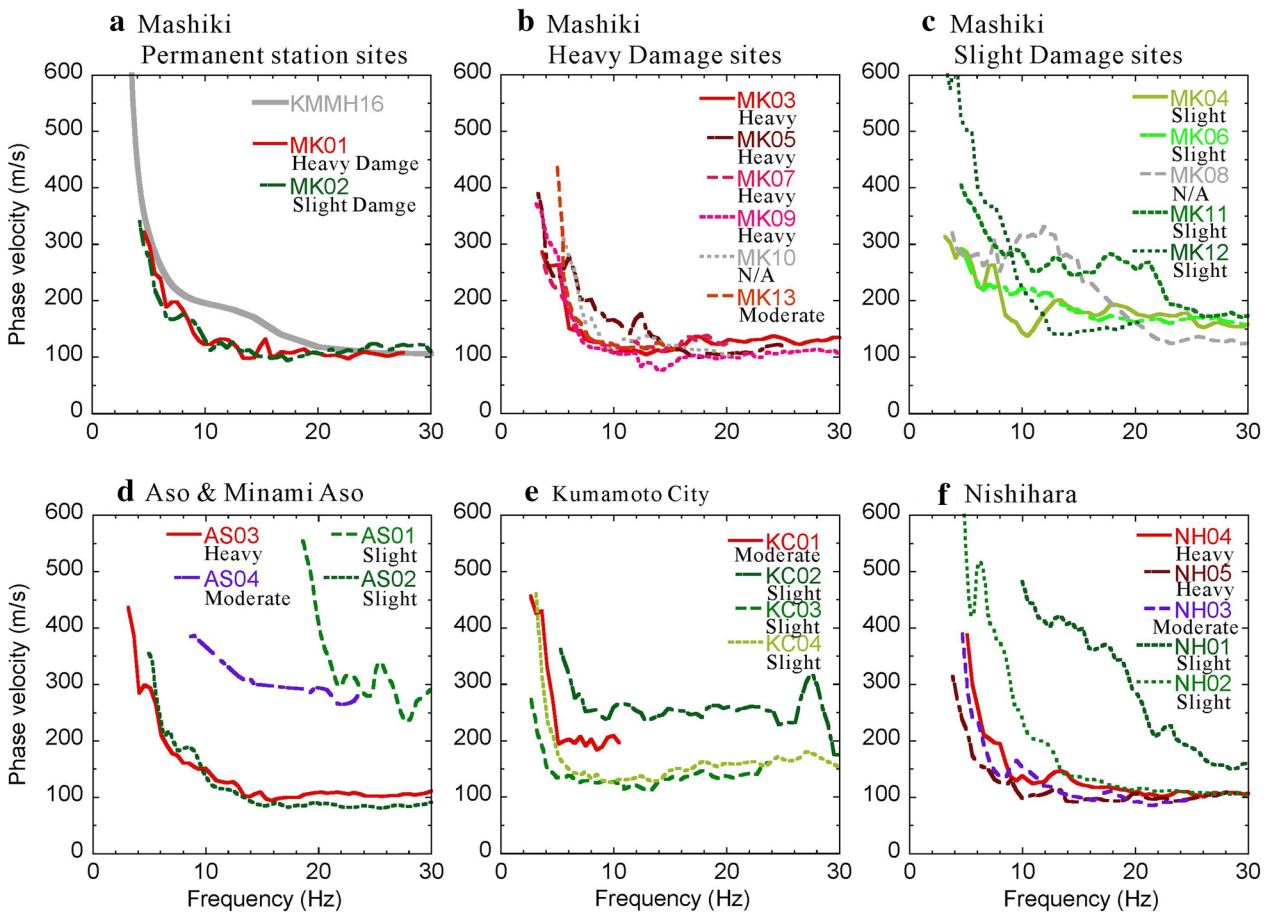

Fig. 2 Phase velocity dispersion curves in Mashiki (**a**–**c**), Aso and Minamiaso (**d**), Kumamoto (**e**) and Nishihara (**f**). The *gray line* in (**a**) shows the calculation results for the model obtained at KMMH16 from borehole logs. In each plot, *warm* and *cool colors* correspond to sites experiencing heavy and light damage, respectively

The soil model for the inversion consisted of a two-layer deposit overlaying an engineering bedrock with an S-wave velocity of 500 m/s, as shown in the shallow soil profile provided at KMMH16. During the inversion, the S-wave velocities in the layers and the interface depths were changed while the V_P-to-V_S ratio in each layer remained fixed at $\sqrt{3}$. This V_P-to-V_S ratio was also obtained based on profiles provided at KMMH16. The density in each layer was also fixed at a constant value determined from the profiles obtained at KMMH16. Examples of the search areas for V_S and the thickness used at most of the sites, such as MK01, are shown in Table 2. The search areas for V_S were variable depending on the dispersive features.

Figure 3a compares the observed phase velocity curve and that calculated for the best-fit model at MK01. Since the technique used in the inversion generates a large number of models during the inversion, many models can be candidates for obtaining the observed phase velocity curve. Therefore, the acceptable phase velocity curves, which differ by 1% from the curve that best fits the observation, were plotted. These acceptable curves are plotted as thin solid lines in Fig. 3a. Although many curves are plotted, the differences between the curves are difficult to observe because the curves are almost identical. The models of the best-fit and acceptable phase velocity curves are shown in Fig. 3b. The difference between the best-fit model and each acceptable model is observable, especially at the depth of the second layer. However, the difference is small and well distributed around the best-fit model. This means the best-fit model was determined prevented from the non-uniqueness problem.

Table 2 Search area used in most sites for inversion analysis

Layer	Density (g/cm^3)	V_p (m/s)	V_S (m/s)	Thickness (m)
1	1.6	$\sqrt{3}\,V_S$	70–150	1–50
2	1.8	$\sqrt{3}\,V_S$	150–500	1–50
3	1.9	1180	500	–

Figure 4 includes plots of the V_S profiles that give the best-fit phase velocity curve. Most sites contain an uppermost (first) layer with low V_S (100–150 m/s). An underlying (second) layer with V_S ranging from approximately 200–300 m/s was found at most sites and reached a depth of approximately 30 m. Figure 4a compares V_S profiles from two permanent strong motion station sites, MK01 and MK02. The slight difference in the second layer between the sites may have been caused by the characteristics of the phase velocity curves at low frequencies. The V_S profile at KMMH16, which is near MK02, was obtained by NIED using suspension logging. The velocities at the two sites were almost identical. However, the uppermost layer is thinner at KMMH16 than at MK02, which may have been caused by the differences between the exact locations of the measurements. The models in Mashiki have a thick first layer with a low V_S of approximately 100 m/s; this layer is especially thick in severely damaged areas, such as those at MK03 and MK09. However, the first layer is not very thick at NH03, which is the permanent strong motion station site in Nishihara (Fig. 4f), and the velocity of the second layer there was lower than that in Mashiki. The V_S profile at AS03, which is located in a heavily damaged district near Aso Bridge, also had a low V_S in the first layer with a depth of 5 m, similar to that in

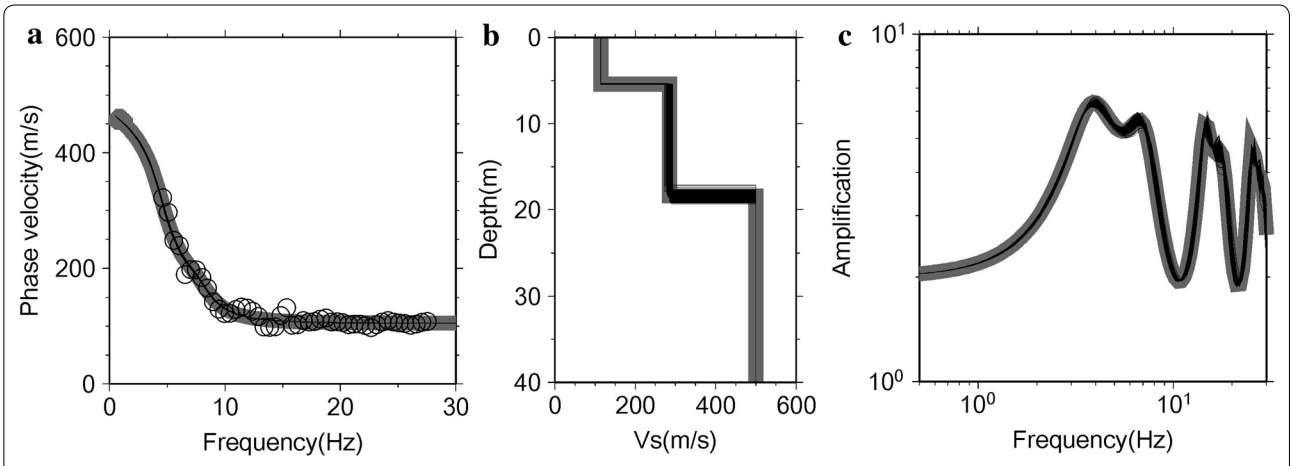

Fig. 3 **a** Observed phase velocity at MK01 (*circles*) and the calculated phase velocity curve for the best-fit model (*gray line*). The curves that differ from the best-fit curve by a maximum of 1% (acceptable curves) are shown as *thin solid lines*. **b** V_S profiles for the best-fit phase velocity curve (*gray*) and acceptable curves (*thin solid line*). **c** Amplification for the best-fit model (*gray*) and acceptable models (*thin solid line*)

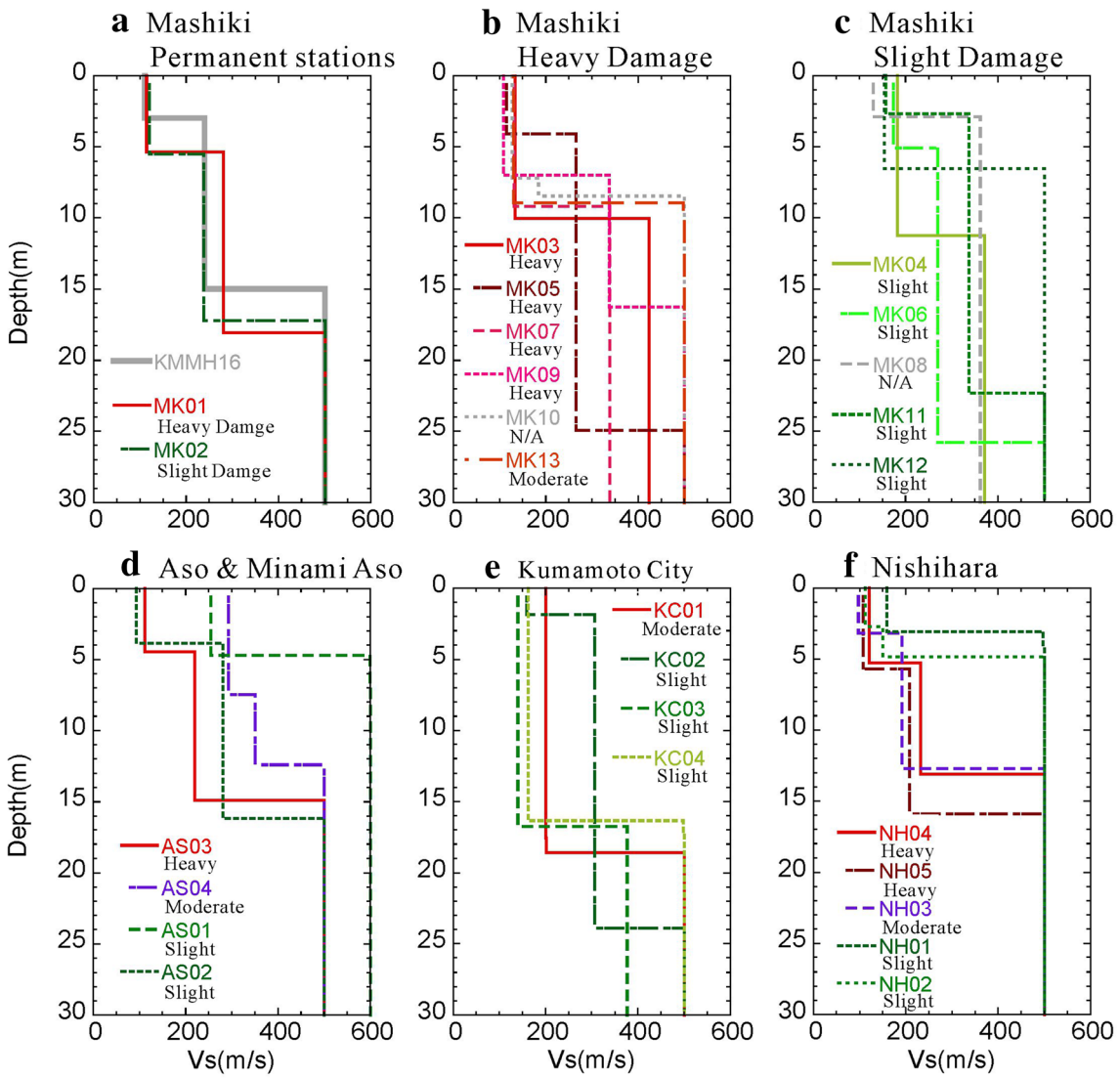

Fig. 4 S-wave velocity profiles estimated from the inversion of the phase velocity in Mashiki (**a**–**c**), Aso and Minamiaso (**d**), Kumamoto (**e**) and Nishihara (**f**). The *line* labeled "KMMH16" represents the results for the model obtained from the borehole logs at the station KMMH16

Mashiki. The first layers of the sites in Kumamoto city are deeper than those in Mashiki except for that at KC02, but their velocities were larger than those in other areas.

Boring logs at several sites in the study area are publicly available online (Japan Geotechnical Consultants Association 2016). The soil properties of the low-velocity first layer that were obtained in this study correspond to those of volcanic ash clay or silt with a small *N*-value of less than 3. This soil layer is distributed on the terrace and lowland in the center of Mashiki. A layer of sand, which has a large *N*-value of greater than 10, may correspond to the second layer profiled in this study, which overlays an engineering bedrock consisting of pumice tuff or gravel.

Average S-wave velocity

Figure 5 illustrates the average S-wave velocities to depths of 5, 10, 20, and 30 m; these are denoted AVS5, AVS10, AVS20, and AVS30, respectively. The velocities were calculated from the detailed V_S profile shown in Fig. 4. As discussed previously, regarding the range of acceptable models in an inversion, the standard deviation of the values of AVS30 obtained for all acceptable models shown in Fig. 3b was evaluated. Since the variation between the acceptable models was small, the standard deviation was also small (Table 1). This indicates that the performance of the inversion was good and the obtained value of AVS30 is reliable. The values of AVS30 obtained at most

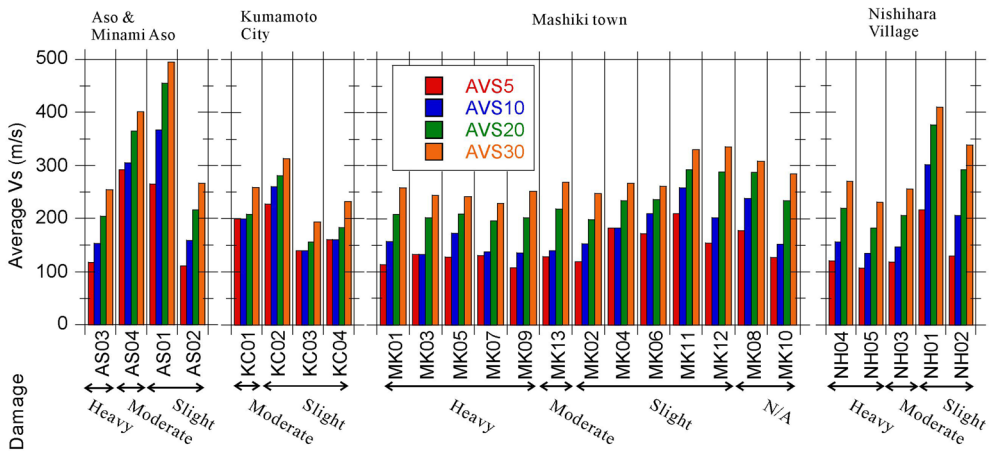

Fig. 5 Average S-wave velocities in the upper 5, 10, 20, and 30 m evaluated from the detailed S-wave velocity profiles with the degree of damage for each site reported by Yamanaka et al. (2016)

of the sites were above approximately 250 m/s (Table 1), corresponding to site soil of type C or D as described by the National Earthquake Hazards Reduction Program (NEHRP), which are defined as "very dense soil and soft rock" and "stiff soil," respectively (Building Seismic Safety Council 2004). No site was classified as NEHRP type E, or "soft soil." Actually, at the severely damaged sites, such as MK01, MK03, and MK09 in Mashiki, the values of AVS30 were similar compared with those at the slightly damaged sites, such as MK04 and MK06, whereas the values of AVS5 were lower than those at the less damaged sites.

AVS30 has been mapped across Japan by the Headquarters for Earthquake Research Promotion (2014) and is available on the website of the Japan Seismic Hazard Information Station (J-SHIS). J-SHIS evaluated AVS30 based on the Japan Engineering Geomorphological Classification Map (Matsuoka et al. 2006). Figure 6 shows a plot of the values of AVS30 extracted from the J-SHIS website and evaluated based on the microtremors observed in this study. In any type of geomorphology, the values of AVS30 evaluated from microtremors in the present study showed values similar to those obtained by J-SHIS at most of the sites.

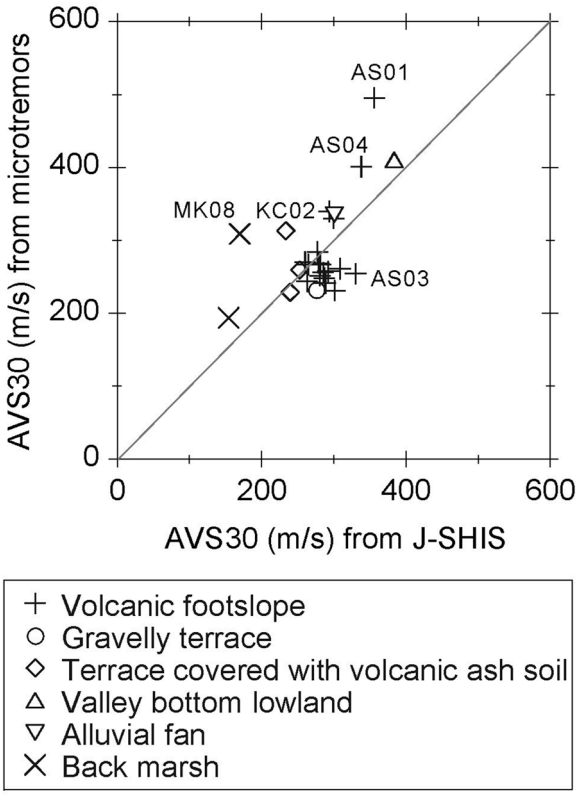

Fig. 6 Comparison of AVS30 values between that evaluated from the microtremor array exploration and that provided from the online by J-SHIS which is evaluated based on the Japan Engineering Geomorphological Classification Map (Matsuoka et al. 2006)

Discussion

Site response characteristics

The site amplifications were compared using the horizontal component of the S-waves assuming one-dimensional vertically incident propagation from the engineering bedrock. Since insufficient information about the quality factor of shallow soil in this region was available, it was assumed to be one-fifth of V_S (in m/s). Figure 3c demonstrates the influence of the difference between the acceptable models on the amplification. This also confirms that the differences between the acceptable models do not have a significant effect on the amplification

and therefore the amplification calculated for the best-fit model is reliable. Figure 7a compares the amplifications of the best-fit models at the two strong motion stations MK01 and MK02. The amplifications at these sites do not differ significantly from one another, as can be inferred from the similarity in their V_S profiles. A peak occurred at 3–4 Hz with a maximum amplification of between approximately 6 and 7. The amplification at KMMH16 is also plotted as a reference. The amplification at KMMH16 cannot simply be compared with that at MK01 and MK02, since the profile at KMMH16 reaches the deep layer with a V_S of 2700 m/s. The influence of deep layers will be discussed later. The first peak occurred at 3–4 Hz at MK09, NH03, and AS03 (Fig. 7b). The maximum amplification was largest at MK09, which is one of the sites in Mashiki that experienced the heaviest damage. At KC03, located in the southern part of Kumamoto city, the first peak appeared at a lower frequency than at the other sites because of the deep soft soils. Yamanaka et al. (2016) used MK06 as a reference site for a site effect study in Mashiki. However, even though the amplification at MK06 is smaller than that at the other sites, the ground motion can be amplified in the frequency range above 1 Hz. This effect must be removed in future studies of the site effects if MK06 is used as a reference.

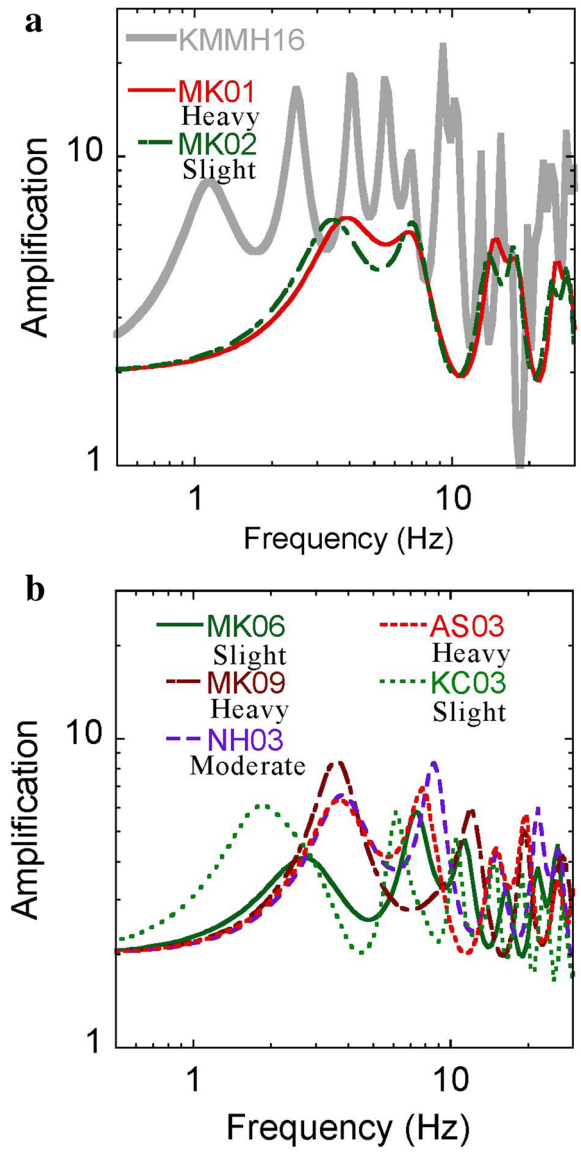

Fig. 7 Site amplification factor for the horizontal component of S-waves assuming one-dimensional vertically incident propagation from the engineering bedrock at two permanent station sites (**a**) and other sites (**b**). The *gray line* in (*a*) shows the computed results for the model at KMMH16

The amplification factors were averaged over the period range of 0.1–2.5 s. The range was defined as the same range with spectral intensity. The average S-wave velocities at the considered depths are plotted against the mean amplification factors in Fig. 8. AVS5 and AVS10 showed a high correlation with the average amplification. This means that the S-wave velocity in the top several meters is a better proxy than AVS30 for site amplification evaluation at the damaged sites. The results of the numerical analysis of the amplification can be confirmed in future work using the actual observation records obtained by Yamanaka et al. (2016).

Influence of deep sedimentary layers

Thus far, this paper has discussed the investigation of the shallow S-wave velocity structure. In general,

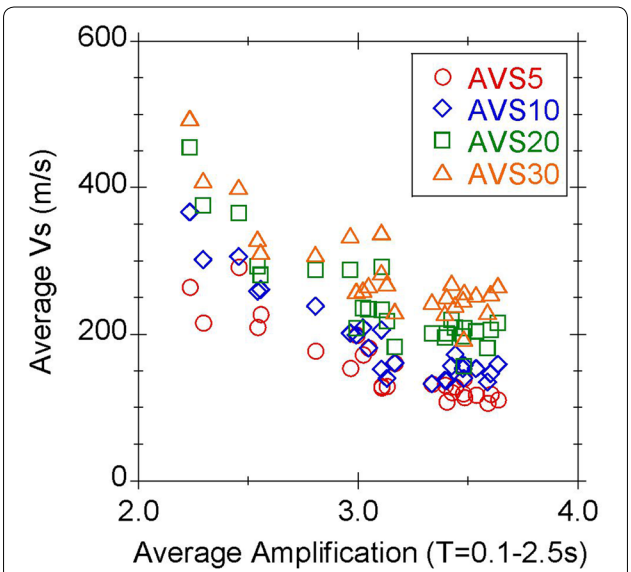

Fig. 8 Average S-wave velocity in the top 5, 10, 20, and 30 m plotted against the amplification averaged over the period range of 0.1–2.5 s

sediment-induced amplification is controlled by the impedance contrast between the near-surface layers and the depth to basement when the velocity exceeds 3 km/s. Figure 9 demonstrates the effect of deep sedimentary layers on the phase velocity dispersion curve and the horizontal-to-vertical spectral ratio (H/V). As mentioned above, the model at KMMH16 does not match the observed phase velocity curve even though the model consists of shallow and deep sedimentary layers. However, the replacement V_S model in the shallow part of the V_S structure determined from microtremors compares favorably with the observation. This means that the deep sedimentary layers are not sensitive to the phase velocity curve in the range above approximately 4 Hz as long as the deep sedimentary layers are similar to those at KMMH16. However, the effect of the deep sedimentary layers on the H/V of the microtremors is significant. The observed H/V curve was estimated from the horizontal and vertical microtremors, which were simultaneously recorded at the center of the array exploration at KMMH16. The synthetic H/V was assumed to follow the ellipticity of fundamental-mode Rayleigh waves. Figure 9 clearly shows that the features of the observed H/V cannot be described using only the shallow V_S profile, indicating the shallow soil is insufficient to explain the H/V. Future investigations of the site effects in the region should therefore include observation of the deep sedimentary layers for the evaluation of the amplification factor over a broad frequency range, as previously discussed with regard to the site response characteristics shown in Fig. 7a.

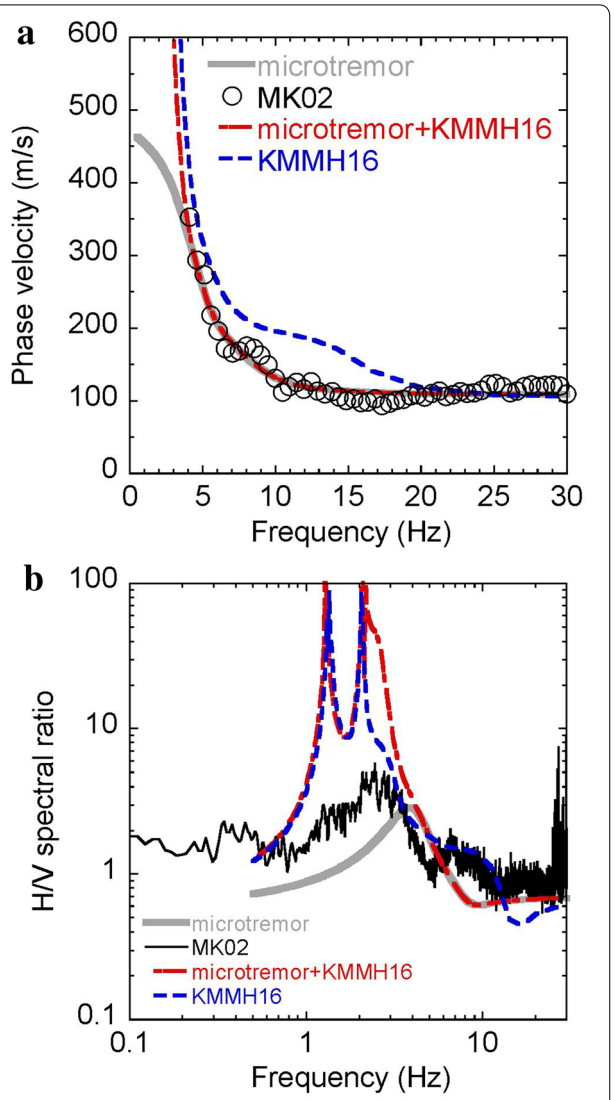

Fig. 9 **a** Comparison of observed phase velocity curves (*circles*) with those calculated for the model at KMMH16 (*blue*), for the shallow V_S model determined from the observed microtremors (*gray*), and for the replacement V_S model in the shallow part of the V_S structure determined from the observed microtremors (*red*). **b** Same comparison as in (**a**) for the H/V

Influence of temporal velocity change

After the 2011 Tohoku earthquake, the velocity of shallow soil was decreased about 5% and it took more than a month to recover the S-wave velocity (Nakata and Snieder 2011). Figure 10 shows the influence of velocity decreases on the phase velocity, because it is unknown that how much velocity change occurred due to the 2016 Kumamoto earthquake and how long did it take to recover from the change. It is noted that the phase velocity curve does not change much even if the velocity of 5% decrease was not recovered at the moment for the measurement of microtremors. This means that even if the velocity has been decreased 5%, it is not detectable by the inversion analysis considering the fluctuation for observed phase velocity. However, if the velocity was decreased 10% at the moment, the difference is clear between the observation and theoretical phase velocity. This implies that even there was a slight velocity change with the percentage of below 5% during the measurement, it does not affect to the *Vs* profiling. But it is noted that if the velocity was about 10% smaller, then it must be detectable in the inversion analysis. Considering the consistency between our result and *Vs* profile provided at the KMMH16 (Fig. 4a), it is clear that there was no significant velocity decrease at the moment for the measurement of microtremors.

Conclusions

Shallow V_S profiles were estimated using microtremor array exploration at temporary strong motion observation stations deployed to record the aftershocks of the 2016 Kumamoto earthquake. The shallow V_S profiles of

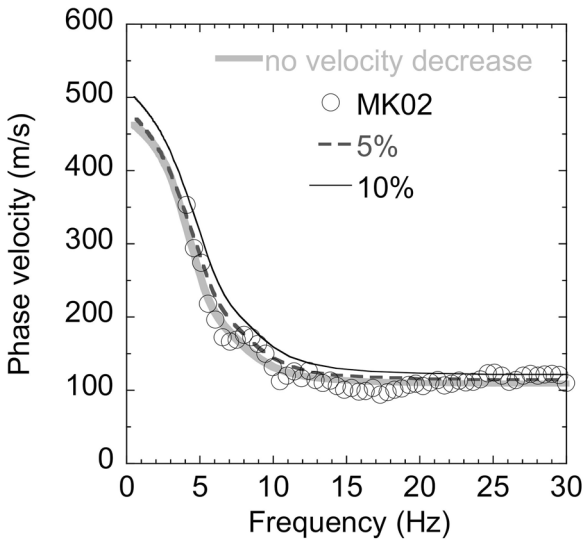

Fig. 10 Influence of velocity change on phase velocity curve. Theoretical dispersion curves were calculated for the V_S profiles which were estimated by assuming no velocity change (*light gray*; same as that shown in Fig. 9a), and for the V_S profiles which were recovered from the temporal velocity decreases with 5% (*broken gray*) and 10% (*thin black*) at the moment for the measurement. The observed phase velocity is also plotted by *circle* which is same as that shown in Fig. 9a

two permanent strong motion station sites in Mashiki were almost identical. The uppermost layer, which had a low V_S of approximately 100 m/s, was widely distributed in Mashiki, Nishihara, and the western Aso area. The thickness of this layer was greater than 5 m in the areas that suffered severe damage. This layer greatly contributes to the amplification factor in the period range of 0.1–2.5 s, as indicated by the fact that AVS5 and AVS10 showed a better correlation with the average amplification factor than AVS30 did. Although the shallow V_S profiles fit well with the observed phase velocity curve in the high frequency range, the deep sedimentary layers were found to have a significant influence on the H/V. Attention must be paid to interpret H/V by using only the shallow V_S structure. Further work should include the influence of deep sedimentary layers for future site amplification studies covering a broad frequency range.

Authors' contributions

KC and HY analyzed the microtremor data and drafted the manuscript. All the authors participated in the measurement of microtremors and edited the manuscript. All authors read and approved the final manuscript.

Author details

[1] Tokyo Institute of Technology, Tokyo, Japan. [2] Railway Technical Research Institute, Tokyo, Japan. [3] The University of Tokyo, Tokyo, Japan. [4] University of Teacher Education Fukuoka, Fukuoka, Japan.

Acknowledgements

We thank those who supported microtremor measurements. This work was partly supported by the Grant-in-Aid for Special Purposes (16H06298: P.I. Hiroshi Shimizu). We used the soil profiles at KMMH16 provided by NIED. We thank the editor and two anonymous reviewers who helped to improve the manuscript.

Competing interests

The authors declare that they have no competing interests.

Received: 29 July 2016 Accepted: 3 December 2016
Published online: 19 December 2016

References

Borcherdt RD (1970) Effects of local geology on ground motion near San Francisco Bay. Bull Seismol Soc Am 60:29–61

Building Seismic Safety Council (2004) NEHRP recommended provisions for seismic regulations or new buildings and other structures, 2003 edn., vol 450. Federal Emergency Management Agency, Washington

Editorial Meeting of Geologic map of Kumamoto (2008) Geologic map of Kumamoto; 253 scale 1:100.000. Kumamoto Geotechnical Consultants Association, Fuji Micro Corp, Kumamoto

Grutas R, Yamanaka H (2012) Shallow shear-wave velocity profiles and site response characteristics from microtremor array measurements in Metro Manila, Philippines. Explor Geophys 43:255–266

Hobiger M, Wegler U, Shiomi K, Nakahara H (2016) Coseismic and post-seismic velocity changes detected by passive image interferometry: comparison of one great five strong earthquakes in Japan. Geophys J Int 205:1053–1073

Japan Geotechnical Consultants Association (2016) Emergency open site for boring logs for reconstruction assistance after the 2016 Kumamoto earthquake. http://geonews.zenchiren.or.jp/2016KumamotoEQ/index.html. Accessed 28 Jun 2016

Kudo K, Kanno T, Okada H, Ozel O, Erdik M, Sasatani T, Higashi S, Takahashi M, Yoshida K (2002) Site-specific issues for strong ground motions during the Kocaeli, Turkey, earthquake of 17 August 1999, as inferred from array observations of microtremors and aftershocks. Bull Seismol Soc Am 92:448–465. doi:10.1785/0120000812

Matsuoka M, Wakamatsu K, Fujimoto K, Midorikawa S (2006) Average shear-wave velocity mapping using Japan engineering geomorphologic classification map. Struct Eng Earthq Eng JSCE 23:57–68

Nakata N, Snieder R (2011) Near-surface weakening in Japan after the 2011 Tohoku-Oki earthquake. Geophys Res Lett 38:L17302

Okada H (2003) The microtremor survey method. Geophysical monograph series No. 12. Society of Exploration Geophysicists, Tulsa

Pavlenko OV, Irikura K (2006) Nonlinear behavior of soils revealed from the records of the 2000 Tottori, Japan, earthquake at stations of the digital strong-motion network Kik-Net. Bull Seismol Soc Am 96:2131–2145

Sawazaki K, Sato H, Nakahara H, Nishimura T (2009) Time-lapse change of seismic velocity in the shallow ground caused strong ground motion shock of the 2000 Western-Tottori earthquake, Japan, as revealed from coda deconvolution analysis. Bull Seismol Soc Am 99:352–366

Takekoshi M, Yamanaka H (2009) Waveform inversion of shallow seismic refraction data using hybrid heuristic search method. Explor Geophys 40:99–104

Takeyama K, Hisada T, Ohsaki Y (1960) Behaviour and design of wooden buildings subjected to earthquakes. In: Proceedings on 2nd WCEE, Tokyo, pp 2093–2111

The Headquarters for Earthquake Research Promotion (2014) Japan seismic hazard information station ver. 2014. http://www.j-shis.bosai.go.jp/map/. Accessed 01 Jun 2016

Yamanaka H (2007) Inversion of surface-wave phase velocity using hybrid heuristic search method. Butsuri Tansa 60:265–275. doi:10.3124/segj.60.265 **(in Japanese)**

Yamanaka H, Chimoto K, Miyake H, Tsuno S, Yamada N (2016) Observation of earthquake ground motion due to aftershocks of the 2016 Kumamoto earthquake in damaged areas. Earth Planets Space 68:197. doi:10.1186/s40623-016-0574-2